Chinese Journal of
POLYMER SCIENCE

RESEARCH ARTICLE

https://doi.org/10.1007/s10118-022-2683-7
Chinese J. Polym. Sci. **2022**, *40*, 1006–1015

Controlling Membrane Phase Separation of Polymersomes for Programmed Drug Release

Shuai Chen[a,b], Erik Jan Cornel[b], and Jian-Zhong Du[a,b*]

[a] *Department of Orthopedics, Shanghai Tenth People's Hospital, School of Medicine, Tongji University, Shanghai 200072, China*
[b] *Department of Polymeric Materials, School of Materials Science and Engineering, Tongji University, Shanghai 201804, China*

Electronic Supplementary Information

Abstract Programmed release of small molecular drugs from polymersomes is of great importance in drug delivery. A significant challenge is to adjust the membrane permeability in a well-controlled manner. Herein, we propose a strategy for controlling membrane phase separation by photo-cross-linking of the membrane-forming blocks with different molecular architectures. We synthesized three amphiphilic block copolymers with different membrane-forming blocks, which are poly(ethylene oxide)$_{43}$-*b*-poly((ε-caprolactone)$_{45}$-*stat*-((α-(cinnamoyloxymethyl)-1,2,3-triazol)caprolactone)$_{25}$) (PEO$_{43}$-*b*-P(CL$_{45}$-*stat*-CTCL$_{25}$)), PEO$_{43}$-*b*-P(CL$_{108}$-*stat*-CTCL$_{16}$), and PEO$_{43}$-*b*-PCTCL$_4$-*b*-PCL$_{79}$. These polymers were self-assembled into polymersomes using either a solvent-switch or powder rehydration method, and the obtained polymersomes were characterized by dynamic light scattering and transmission electron microscopy. Then the phase separation patterns within the polymersome membranes were investigated by mesoscopic dynamics (MesoDyn) simulations. To further confirm the change of the membrane permeability that resulted from the phase separation within the membrane, doxorubicin, as a small molecular drug, was loaded and released from the polymersomes. Due to the incompatibility between membrane-forming moieties (PCTCL and PCL), phase separation occurs and the release rate can be tuned by controlling the membrane phase pattern or by photo-cross-linking. Moreover, besides the compacting effect by formation of chemical bonds in the membrane, the cross-linking process can act as a driving force to facilitate the rearrangement and re-orientation of the phase pattern, which also influences the drug release behavior by modulating the cross-membrane distribution of the amorphous PCTCL moieties. In this way, the strategy of focusing on the membrane phase separation for the preparation of the polymersomes with finely tunable drug release rate can be envisioned and designed accordingly, which is of great significance in the field of delivery vehicles for programmed drug release.

Keywords Polymersome; Drug delivery; Phase separation; Programmed drug release

Citation: Chen, S.; Cornel, E. J.; Du, J. Z. Controlling membrane phase separation of polymersomes for programmed drug release. *Chinese J. Polym. Sci.* **2022**, *40*, 1006–1015.

INTRODUCTION

Drug delivery is important and necessary in various cancer therapies and other hard-to-cure diseases.[1,2] However, it is still an important challenge to achieve both effective and efficient delivery in practice, owing to the insufficient control over the drug release process.[3–5] Polymersomes have membrane barriers and enclosed lumens, which serve as a promising and versatile platform in drug delivery.[6–8] However, due to the homogeneity of conventional polymersome membranes, the release of drug is hard to control, leading to inefficient disease treatment.[9]

Despite the diversified effecting mechanisms of drugs, most drugs are required to be released from their delivery vehicles and reach a certain concentration locally or systemically during the process of treatment.[10–13] Through a careful control over the drug release procedures, the polymersomes can deliver drug in a more customized way to meet with the demands of biomedical practices, which is also known as programmed drug delivery.[14–16]

An important method to allow programmed release of small molecular drugs is to carefully adjust the properties of the polymersome membrane.[17–19] Generally, the membrane permeability of polymersomes can be altered by designing various specific polymersome membranes, introducing specific targeting functional groups, or by preparing biohybrid polymersomes.[20–23] For example, the change in membrane thickness,[24,25] cross-linking density,[26–28] or insertion of transmembrane proteins[29,30] have shown to significantly affect the drug release rate. Recently, the development of polymersomes with inhomogeneous membranes has drawn considerable attention.[31] They can be modularly-designed and meet biomedical requirements,[32] such as control of blood sugar,[33] facile loading and release of macromolecules,[34,35] visualization of antimicrobial process,[36] and so forth. These

* Corresponding author, E-mail: jzdu@tongji.edu.cn
Special Issue: Biomedical Polymers
Received October 21, 2021; Accepted December 14, 2021; Published online February 23, 2022

polymersomes consist of an inhomogeneous membrane with multiple phases.[9] Orchestrating the distribution of phases with different permeabilities would make such polymersomes relevant for the development of the next generation of programmed drug delivery vehicles. Unfortunately, a universal method to conveniently adjust membrane permeability that utilizes phase separation has not yet been developed.

We have previously reported two principles to acquire polymersomes with ultrahigh biomacromolecular loading efficiencies, namely: 'acid-induced adsorption' and 'affinity-enhanced attraction'.[27] This report was based on poly(ethylene oxide)-*b*-poly((*α*-(cinnamoyloxymethyl)-1,2,3-triazol)caprolactone) (PEO-*b*-PCTCL). The polymersome membrane composed of such a PCTCL block remains biodegradable even when photo-cross-linked. This aspect shows promising potential for *in vivo* drug delivery by achieving a balance between stability and degradability. However, the amorphous character of PCTCL makes the membrane extremely permeable to small molecules, which in turn renders the polymersome inefficient to deliver small molecules for broader applications.

Herein, to meet this challenge, poly(ε-caprolactone) (PCL) was introduced to prepare semi-crystalline polymersome membranes that are less permeable than the previously reported PCTCL membranes, making them more suitable for broader applications such as programmed drug release. More specifically, better control over the small molecule release rate was achieved by judicious control of the membrane phase separation (Scheme 1). This was achieved by preparing phase-separated membranes from copolymers with statistical compositions or a block composition, additionally photo-cross-linking was used to further modify the phase separation within the membrane. Three polymers with different architectures of membrane-forming blocks were prepared and self-assembled into polymersomes: PEO_{43}-*b*-P(CL_{45}-*stat*-$CTCL_{25}$), PEO_{43}-*b*-P(CL_{108}-*stat*-$CTCL_{16}$), and PEO_{43}-*b*-$PCTCL_4$-*b*-PCL_{79}. Owing to the incompatible nature between the semi-crystalline PCL and amorphous PCTCL moieties, phase separation occurs within the compacted polymersome membrane. The phase separation patterns were simulated by mesoscopic dynamics (MesoDyn) method and the drug release behavior was predicted accordingly, and these predictions were confirmed by a series of drug release tests. The above proposed strategy was confirmed to effectively manipulate the release of small molecular drug from the polymersomes, which is also of great potency in the future development of programmed drug delivery vehicles.

EXPERIMENTAL

Synthesis of PEO_{43}-*b*-P(CL_{45}-*stat*-$CTCL_{25}$)

Synthesis of PEO_{43}-b-P[CL_{45}-stat-(aClCL)$_{25}$]

First, PEO_{43} (0.800 g, 0.421 mmol) and ε-caprolactone (2.43 g, 21.1 mmol) were dissolved in toluene (150 mL) under stirring. Then, the solution was azeotropically distilled at 130 °C to remove approximately 50 mL of solvent, afterwards *α*-chlorocaprolactone (1.88 g, 12.7 mmol) was quickly added at the same temperature. Distillation was continued and after removal of the following solvent fraction (approximately 80 mL), the reaction was cooled to room temperature and degassed with argon for 25 min. Subsequently, stannous octoate (6.0 mg, 0.015 mmol) was added and the mixture was degassed with argon for

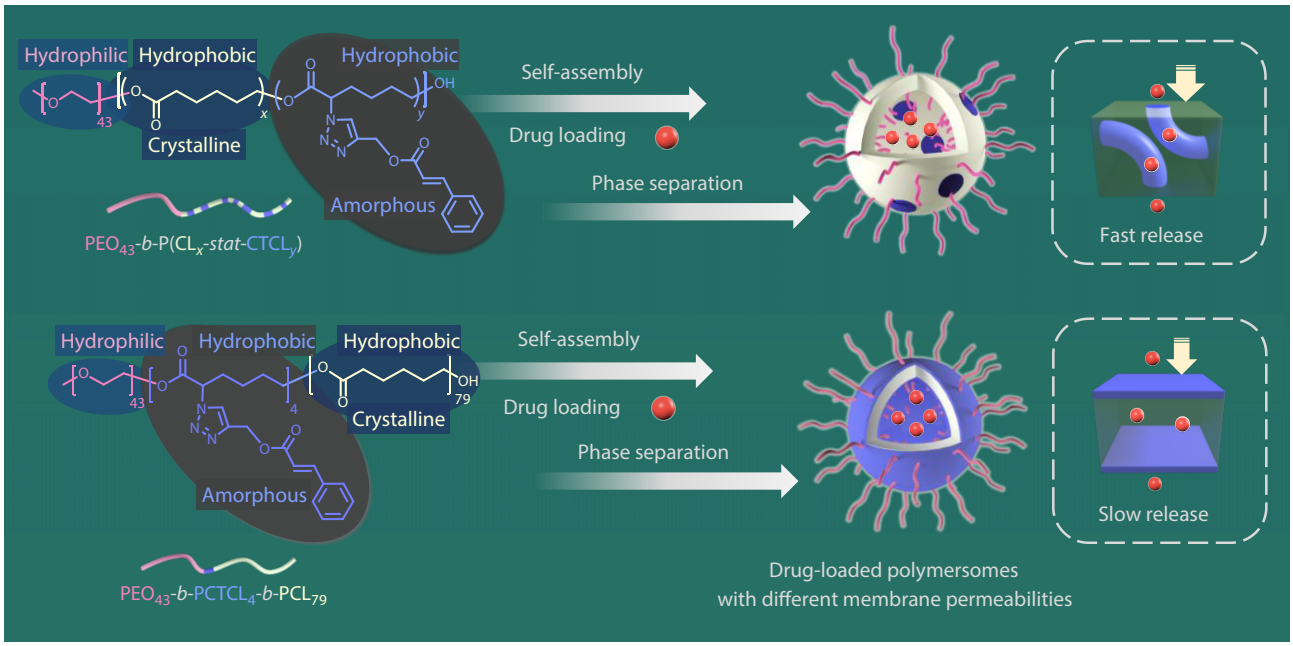

Scheme 1 Controlling phase separation of polymersome membrane for tuning membrane permeability and drug release rate. Amphiphilic copolymers with different membrane-forming blocks consisting incompatible moieties were synthesized, which lead to different phase patterns after self-assembly. Small molecular drugs can be loaded during self-assembly. Owing to the inherent permeability difference between semi-crystalline PCL and amorphous PCTCL, the membrane permeability can be tuned according to the phase patterns, thus tuning the drug release rate. The polymersomes with connected PCTCL phases release drugs faster than those with a continuous PCL shell within the membrane.

https://doi.org/10.1007/s10118-022-2683-7

another 15 min to remove oxygen. The reaction was then heated to 110 °C and stirred for 48 h under an argon atmosphere. Afterwards, the crude reaction mixture was cooled to room temperature and concentrated *in vacuo*. The crude product was dissolved into dichloromethane (10 mL) and precipitated in cold petroleum ether (200 mL). Precipitation was repeated twice and the final product was dried *in vacuo* at 25 °C until a constant weight was achieved (yield: 82%).

Synthesis of PEO_{43}-b-P[CL_{45}-stat-(N_3CL)$_{25}$]

PEO_{43}-*b*-P[CL_{45}-*stat*-(*α*ClCL)$_{25}$] (2.00 g, containing 4.65 mmol of chlorine) was first dissolved in *N*,*N*-dimethylformamide (DMF, 20 mL) under magnetic stirring. Then, an excess amount of NaN_3 (1.51 g, 23.2 mmol) was added and the reaction was stirred at room temperature for 24 h. Dichloromethane (40 mL) was added to the crude mixture to induce precipitation of NaN_3 and NaCl. After filtration, the mixture was washed for three times with deionized water, and dried overnight with adequate amount of anhydrous $MgSO_4$. The mixture was subsequently filtered and concentrated *in vacuo* until approximately 10 mL remained. The product was precipitated twice in cold petroleum ether (2×200 mL) and dried afterwards *in vacuo* at 25 °C until a constant weight was achieved (yield: 75%).

Synthesis of PEO_{43}-b-P(CL_{45}-stat-$CTCL_{25}$)

PEO_{43}-*b*-P[CL_{45}-*stat*-(N_3CL)$_{25}$] (1.00 g, containing 2.29 mmol of azide group), propargyl cinnamate (0.838 g, 4.50 mmol), and *N*,*N*,*N*′,*N*″,*N*″-pentamethyldiethylenetriamine (PMDETA, 62 μL, 0.30 mmol) were mixed and fully dissolved in tetrahydrofuran (THF, 20 mL). Then the solution was degassed with argon for 25 min before addition of CuBr (43.2 mg, 0.300 mmol). After another 15 min of degassing, the reaction was stirred at 50 °C for 36 h. The crude reaction mixture was cooled to room temperature and diluted with THF (30 mL) prior to purification using a column packed with neutral aluminium oxide, using THF as eluent. The solution was then concentrated to approximately 10 mL and precipitated twice in cold petroleum ether (2×200 mL), using dichloromethane (10 mL) as good solvent for the second precipitation step. The final purified product that was dried *in vacuo* at 25 °C until a constant weight was achieved (yield: 85%).

Synthesis of PEO_{43}-*b*-P(CL_{108}-*stat*-$CTCL_{16}$)

Synthesis of PEO_{43}-b-P[CL_{108}-stat-(αClCL)$_{16}$]

First, PEO_{43} (1.30 g, 0.684 mmol) and *ε*-caprolactone (8.36 g, 72.6 mmol) were dissolved in toluene (150 mL) under stirring. Then, the solution was azeotropically distilled at 130 °C to remove approximately 50 mL of solvent, afterwards *α*-chloro-caprolactone (1.63 g, 10.9 mmol) was quickly added at the same temperature. Distillation was continued and after removal of a following solvent fraction (approximately 80 mL), the reaction was cooled to room temperature and degassed with argon for 25 min. Subsequently, stannous octoate (8.0 mg, 0.020 mmol) was added and the mixture was degassed with argon for another 15 min to remove oxygen. The reaction was then heated to 110 °C and stirred for 48 h under an argon atmosphere. Afterwards, the crude reaction mixture was cooled to room temperature, and concentrated *in vacuo*. The crude product was dissolved into dichloromethane (10 mL) and precipitated in cold petroleum ether (200 mL). Precipitation was repeated twice, and the final product was dried *in vacuo* at 25 °C until a constant weight was achieved (yield: 78%).

Synthesis of PEO_{43}-b-P[CL_{108}-stat-(N_3CL)$_{16}$]

PEO_{43}-*b*-P[CL_{108}-*stat*-(*α*ClCL)$_{16}$] (4.14 g, containing 3.99 mmol of chlorine) was first dissolved in DMF (20 mL) under magnetic stirring. Then, an excess amount of NaN_3 (1.30 g, 20.0 mmol) was added and the reaction was stirred at room temperature for 24 h. Dichloromethane (40 mL) was added to the crude mixture to induce precipitation of NaN_3 and NaCl. After filtration, the mixture was washed for three times with deionized water, and dried overnight with adequate amount of anhydrous $MgSO_4$. The mixture was subsequently filtered and concentrated *in vacuo* until approximately 10 mL remained. The product was precipitated twice in cold petroleum ether (2×200 mL) and dried afterwards *in vacuo* at 25 °C until a constant weight was achieved (yield: 70%).

Synthesis of PEO_{43}-b-P(CL_{108}-stat-$CTCL_{16}$)

PEO_{43}-*b*-P[CL_{108}-*stat*-(N_3CL)$_{16}$] (2.50 g, containing 2.40 mmol of azide group), propargyl cinnamate (0.782 g, 4.20 mmol), and PMDETA (62 μL, 0.30 mmol) were mixed and fully dissolved in THF (20 mL). Then the solution was degassed with argon for 25 min before addition of CuBr (43.2 mg, 0.300 mmol). After another 15 min of degassing, the reaction was stirred at 50 °C for 36 h. The crude reaction mixture was cooled to room temperature and diluted with THF (30 mL) prior to purification using a column packed with neutral aluminium oxide, using THF as eluent. The solution was then concentrated to approximately 10 mL and precipitated twice in cold petroleum ether (2×200 mL), using dichloromethane (10 mL) as good solvent for the second precipitation step. The final purified product that was dried *in vacuo* at 25 °C until a constant weight was achieved (yield: 77%).

Synthesis of PEO_{43}-*b*-P$CTCL_4$-*b*-PCL_{79}

Synthesis of PEO_{43}-b-P(αClCL)$_4$

First, PEO_{43} (2.25 g, 1.18 mmol) was dissolved in toluene (120 mL) under stirring. Then, the solution was azeotropically distilled at 130 °C to remove approximately 40 mL of solvent, afterwards, *α*-chloro-caprolactone (1.90 g, 12.8 mmol) was quickly added at the same temperature. Distillation was continued and after removal of a following solvent fraction (approximately 60 mL), the reaction was cooled to room temperature and degassed with argon for 25 min. Subsequently, stannous octoate (10.0 mg, 0.0247 mmol) was added and the mixture was degassed with argon for another 15 min to remove oxygen. The reaction was then heated to 110 °C and stirred for 48 h under an argon atmosphere. Then, the reaction was cooled to room temperature, and concentrated *in vacuo*. The crude product was dissolved into dichloromethane (10 mL) and precipitated in cold petroleum ether (200 mL). Precipitation was repeated twice and the final product was dried *in vacuo* at 25 °C until a constant weight was achieved (yield: 72%).

Synthesis of PEO_{43}-b-P(αClCL)$_4$-b-PCL_{79}

First, PEO_{43}-*b*-P(*α*ClCL)$_4$ (1.06 g, 0.425 mmol) and *ε*-caprolactone (4.16 g, 36.1 mmol) were dissolved in toluene (100 mL) under stirring. Then, the solution was azeotropically distilled at 130 °C to remove approximately 80 mL of solvent, afterwards, the reaction was cooled to room temperature and degassed with

https://doi.org/10.1007/s10118-022-2683-7

argon for 25 min. Subsequently, stannous octoate (8.0 mg, 0.020 mmol) was added and the mixture was degassed with argon for another 15 min to remove oxygen. The reaction was then heated to 110 °C and stirred for 48 h under an argon atmosphere. Afterwards, the crude reaction mixture was cooled to room temperature, and concentrated *in vacuo*. The crude product was dissolved into dichloromethane (10 mL) and then precipitated in cold petroleum ether (200 mL). Precipitation was repeated twice, and the final product was dried *in vacuo* at 25 °C until a constant weight was achieved (yield: 85%).

Synthesis of PEO_{43}-b-P(N_3CL)$_4$-b-PCL_{79}

PEO_{43}-*b*-P(*α*ClCL)$_4$-*b*-PCL_{79} (2.60 g, containing 0.904 mmol of chlorine group) was first dissolved in DMF (20 mL) under magnetic stirring. Then, NaN_3 (0.294 g, 4.50 mmol) was added and the reaction was stirred at room temperature for 24 h. Dichloromethane (40 mL) was added to the crude mixture to induce precipitation of NaN_3 and NaCl. After filtration, the mixture was washed three times with deionized water, and dried overnight with adequate amount of anhydrous $MgSO_4$. The mixture was subsequently filtered and concentrated *in vacuo* until approximately 10 mL remained. The product was precipitated twice in cold petroleum ether (2×200 mL) and dried afterwards *in vacuo* at 25 °C until a constant weight was achieved (yield: 74%).

Synthesis of PEO_{43}-b-$PCTCL_4$-b-PCL_{79}

PEO_{43}-*b*-P(N_3CL)$_4$-*b*-PCL_{79} (1.70 g, containing 0.590 mmol of azide group), propargyl cinnamate (0.218 g, 1.17 mmol), and PMDETA (21 μL, 0.10 mmol) were mixed and fully dissolved in THF (20 mL). Then the solution was degassed with argon for 25 min before addition of CuBr (14.2 mg, 0.0986 mmol). After another 15 min of degassing, the reaction was stirred at 50 °C for 36 h. The crude reaction mixture was cooled to room temperature and diluted with THF (30 mL) prior to purification using a column packed with neutral aluminium oxide, using THF as eluent. The solution was then concentrated to approximately 10 mL and precipitated in cold petroleum ether (200 mL). Precipitation was further repeated twice and the final product was dried *in vacuo* at 25 °C until a constant weight was achieved (yield: 82%).

Self-assembly of Copolymers into Polymersomes

Solvent-switch method

For each synthesized polymer, 3.0 mg polymer was weighed into a 25 mL vial and diluted with dimethyl sulfoxide (DMSO, 2.0 mL). The polymer was fully dissolved and deionized water (4.0 mL) was added dropwise under stirring, afterwards this dispersion was stirred for 30 min. This dispersion was subsequently dialyzed (using a dialysis tube with a molecular weight cut-off of 14000) using deionized water (1.0 L) for two days (the deionized water was refreshed every 8 h). The final dispersion was stored at room temperature and further analyzed as described below. The same self-assembly procedure was also performed using THF as initial solvent.

Powder rehydration method

For each synthesized polymer, 3.0 mg of polymer was weighed into a 25 mL vial and deionized water (6.0 mL) was added. The mixture was stirred for 24 h at room temperature. After complete dissolution of the polymer powder, the resulting polymersome dispersion was used for further tests.

Simulation of Phase Separation within the Membranes of Polymersomes

All simulations were carried out on the software *Materials Studio 2017*.[37]

Calculation of Flory-Huggins parameters

First, models of repeating units of different polymers (PCL, PCTCL, and PEO) were created. By the module of Synthia, the molecular volume (V_m) and solubility parameter (δ) at 298 K were calculated.[38] Using these input parameters, the Flory–Huggins parameter of each pair of polymers was calculated using the following equation:

$$\chi = \frac{V_{ref}(\delta_i - \delta_j)^2}{RT} \quad (1)$$

where the average molar volume (V_{ref}), the gas constant (R), and the temperature (T, 298 K) were used to calculate the Flory-Huggins parameter (χ).

Calculation of parameters for MesoDyn simulations

The module of MesoDyn adopts parameters for repulsion (P_r) which directly relate to Flory-Huggins parameters by the following equation:

$$P_{r_{ij}} = \chi_{ij} RT \quad (2)$$

where χ_{ij} represents the Flory-Huggins parameter between the two components, i and j.

The characteristic ratio (C) of each polymer can be calculated by the module of Synthia. The following equation was used to convert the actual degree of polymerization (D_p) to the number of repeating units for MesoDyn simulations (N_{meso}).

$$N_{meso} = \frac{D_p}{C} \quad (3)$$

MesoDyn simulations of phase separation within the membrane of polymersome

The MesoDyn simulations were carried out *via* the module of MesoDyn Tools, using the above mentioned input parameters.[39] Here, to simulate the real situation, where multiple membrane-forming polymer chains with various hydrophobic interactions over a long period of time are considered, we used a ten-fold calculated parameter for repulsion in the simulations to fasten the time for equilibration and to simplify the simulation procedures. Other parameters for simulations were used as the following: Number of steps: 10000; Time step: 50.0 ns; Bead diffusion coefficient: 1.0×10^{-7} cm^2·s^{-1}; Grid dimensions: 16.0 nm × 32.0 nm × 32.0 nm.

To simulate the phase patterns resulted from chain motions induced by photo-cross-linking, the simulations were carried out with an additional shear of 1.0×10^{-4} ns^{-1}.

Drug Loading and Release of Polymersomes

Preparation of neutral aqueous solution of doxorubicin

Doxorubicin hydrochloride (5.0 mg) was weighed into a 25 mL vial, then, deionized water (5.0 mL) was added and the powder was fully dissolved upon stirring. Afterwards, the pH of the above aqueous solution was adjusted to 7.4 by addition of 0.5 mol/L NaOH solution. This solution was used in the next step once a constant pH was achieved for 0.5 h. The final exact concentration was obtained by correcting for the added amount of NaOH solution.

Loading of doxorubicin into polymersomes

For each synthesized polymer, the polymer powder (4.0 mg) was weighed into a vial and THF (2.0 mL) was added to fully dissolve the powder under magnetic stirring. The doxorubicin solution (pH 7.4) was added, so that the total amount of doxorubicin was 2.0 mg in each case, afterwards deionized water (4.0 mL) was added dropwise. The drug-loaded polymersome dispersion was stirred for an additional 3 h to achieve a final equilibrium. This dispersion was subsequently dialyzed (using a dialysis tube with a molecular weight cut-off of 14000) using deionized water (1.0 L) for 2.5 h (the deionized water was refreshed every 0.5 h). The final dispersion was stored at room temperature and further used in release tests.

Release of doxorubicin from polymersomes

Three portions of 80 mL of Tris buffer (0.01 mol/L, pH 7.4) were added to three 100 mL beakers covered with aluminium foil and heated to 37 °C. Then, 2.0 g of each drug-loaded polymersome dispersions were dialyzed in this solution under stirring. The solution in each beaker was tested at fixed time intervals to quantify the total amount of drug release *via* fluorescence spectroscopy. The amount of released drug was converted to cumulative drug release percentage and recorded against time.

Calculation of drug loading efficiency (DLE)

The fluorescence intensity of samples after each loading experiment was analyzed and compared with a calibration curve of doxorubicin in water, to obtain the doxorubicin concentration in the loaded polymersomes. The corresponding drug loading efficiency was calculated using the following equation:

$$\mathrm{DLE} = \frac{cV}{m_{\mathrm{total}}} \times 100\% \quad (4)$$

where c and V represent the concentration of doxorubicin and the volume of drug-loaded polymersome dispersion, and m_{total} represents the total amount of doxorubicin added initially for the loading experiments.

Characterization

Proton nuclear resonance spectroscopy (^{1}H-NMR)

Experiment were carried out on a Bruker AV 400 MHz or a Bruker Avance NEO 600 NMR spectrometer. The solvent was $CDCl_3$ with tetramethylsilane (TMS) as internal standard.

Size exclusive chromatography (SEC)

Experiment were performed on an Agilent Technologies 1200 Series or Agilent PL-GPC50 size exclusive chromatograph equipped with a set of Waters Styragel chromatographic columns at 25 °C. The mobile phase was DMF and the flow rate was 1.0 mL·min^{-1}.

Dynamic light scattering (DLS)

Experiment were performed on a Malvern ZS-90 Zetasizer. Polystyrene cuvettes were used and the scattering angle was fixed at 90°, all tests were repeated 3×10 times.

Transmission electron microscopy (TEM)

Images were recorded using a JEOL JEM-2100F or HITACHI TEM H-800 microscope, with an acceleration voltage of 220 kV. Samples were diluted to 0.2 mg·mL^{-1}, and 10 μL of this diluted dispersion was dropped onto a carbon-coated copper grid. The sample was frozen at −20 °C and dried under vacuum. Then, 1% of phosphotungstic acid solution (pH 7.0) was used as stain. After 60 s of staining, the stain solution was carefully removed using filter paper.

Fluorescence spectroscopy

A Thermo Scientific Lumina Spectrometer was used with a quartz cuvette, 1.5 mL of sample solution was measured each time. Acetone was used to rinse the cuvette prior to each test. The excitation wave length was set to 461 nm and the emission wave length was set to 591 nm when determining the doxorubicin concentration. The photomultiplier tube voltage was set to 800 V and the integral time was 20 ms.

RESULTS AND DISCUSSION

Synthesis and Characterization of Polymers

Synthesis of PEO_{43}-b-P(CL_{45}-stat-$CTCL_{25}$)

The synthetic route is illustrated in Fig. S1 (in the electronic supplementary information, ESI). First, the monomethylated PEO_{43} was used to initiate the ring-opening polymerization of two caprolactone monomers (ε-caprolactone and α-chloro-caprolactone) to afford PEO_{43}-*b*-P[CL_{45}-*stat*-(α$ClCL)_{25}$]. Then, this polymer went through a click reaction by subsequently reacting with sodium azide and propargyl cinnamate to finally afford PEO_{43}-*b*-P(CL_{45}-*stat*-$CTCL_{25}$). The chemical structures were confirmed by ^{1}H-NMR spectroscopy, and the degree of polymerization was confirmed to be 45 and 25, for CL and α$ClCL, respectively. The chemical compositions of PEO_{43}-*b*-P[CL_{45}-*stat*-($N_3CL)_{25}$] and PEO_{43}-*b*-P(CL_{45}-*stat*-$CTCL_{25}$) were confirmed by ^{1}H-NMR spectroscopy (Figs. S2–S4 in ESI).

The number-averaged molecular weight (M_n) and its polydispersity ($Đ$) were obtained from SEC analysis (Table S1 in ESI). The M_n of PEO_{43}-*b*-P[CL_{45}-*stat*-(α$ClCL)_{25}$] was 3000 and $Đ$ was 1.24. The M_n of PEO_{43}-*b*-P(CL_{45}-*stat*-$CTCL_{25}$) was 14700 and $Đ$ was 1.33. According to ^{1}H-NMR spectroscopy, the molecular weight of the final copolymer is 15580, which is consistent to the SEC results.

Synthesis of PEO_{43}-b-P(CL_{108}-stat-$CTCL_{16}$)

A similar synthetic route to that of PEO_{43}-*b*-P(CL_{45}-*stat*-$CTCL_{25}$), as described in the previous section, was used. The three polymers: PEO_{43}-*b*-P[CL_{108}-*stat*-(α$ClCL)_{16}$], PEO_{43}-*b*-P[CL_{108}-*stat*-($N_3CL)_{16}$] and PEO_{43}-*b*-P(CL_{108}-*stat*-$CTCL_{16}$) were sequentially synthesized and the chemical composition of each polymer was confirmed by ^{1}H-NMR spectroscopy (Figs. S5–S7 in ESI). The M_n and $Đ$ were obtained from SEC analysis (Table S1 in ESI). The M_n of PEO_{43}-*b*-P[CL_{108}-*stat*-(α$ClCL)_{16}$] was 3400 and $Đ$ was 1.35. The M_n of PEO_{43}-*b*-P(CL_{108}-*stat*-$CTCL_{16}$) was 18600 and $Đ$ was 1.32. According to ^{1}H-NMR spectroscopy, the molecular weight of the final copolymer is 19680, which is consistent to the SEC results.

Synthesis of PEO_{43}-b-$PCTCL_4$-b-PCL_{79}

First, the ring-opening polymerization of α$ClCL was initiated by monomethylated PEO_{43} (Fig. S8 in ESI). Then the resulting polymer was used as the initiator in the ring-opening polymerization of CL. Finally, by using click chemistry, the cinnamate group was introduced to the polymer and the triblock copolymer of PEO_{43}-*b*-$PCTCL_4$-*b*-PCL_{79} was synthesized. According to ^{1}H-NMR spectroscopy (Figs. S9 and S10 in ESI), by referring to the peaks on PEO_{43}, the degree of polymerization of the two membrane-forming blocks (PCTCL and PCL) were 4 and 79, respectively. Furthermore, ^{1}H-NMR spectra were used to further confirm the composition of the final triblock copolymer

https://doi.org/10.1007/s10118-022-2683-7

(Figs. S11 and S12 in ESI). The M_n and $Đ$ were obtained from SEC analysis (Table S1 in ESI). The M_n of PEO_{43}-*b*-P(αClCL)$_4$ was 2100 and $Đ$ was 1.10. The M_n of PEO_{43}-*b*-P(αClCL)$_4$-*b*-PCL_{79} was 11900 and $Đ$ was 1.35. The M_n of PEO_{43}-*b*-$PCTCL_4$-*b*-PCL_{79} was 12800 and $Đ$ was 1.34. According to ^{1}H-NMR spectroscopy, the molecular weight of the final copolymer is 12270, which is consistent with the SEC results.

Self-assembly and Characterization of Polymersomes

After synthesis, the polymers were self-assembled *via* the solvent-switch method or powder rehydration method. The self-assemblies were characterized by DLS and TEM. As Fig. 1 shows, polymersomes formed when using either DMSO or THF as the initial solvent in the solvent-switch self-assembly method. However, during self-assembly, DMSO induced a more swollen membrane due to its larger miscibility with water. This likely led to a larger hydrodynamic diameter (D_h) and polydispersity index (PD).

To make polymersomes more suitable for biomedical applications, polymersomes should be able to form directly in pure water.[40] To test this possibility, first, ^{1}H-NMR spectra were recorded from the polymersomes obtained from the powder rehydration method in deuterium oxide (D_2O) (Figs. S13–S15 in ESI). These spectra were compared to those acquired using $CDCl_3$ as solvent (to dissolve the polymer chains). As expected, the peaks corresponding to the PCL moieties are attenuated due to their low solubility in D_2O. However, there are still significant amounts of dissolved PCL chains in water, since these signals were still clearly observed. We hypothesized that the dissolution of these chains facilitated the dispersion and self-assembly process in pure water. Subsequently, we performed this self-assembly method on a larger scale in deionized water (instead of D_2O). The hydrodynamic diameters of the obtained polymersomes were determined by DLS and interestingly this value increased with the weight percentage of PEO (Fig. S16 in ESI). Furthermore, TEM images also confirmed the formation of polymersomes using the powder rehydration method (Fig. S17 in ESI).

An important aspect of drug delivery vehicles is their stability under physiological conditions. This was evaluated using DLS studies. All the prepared polymersomes were incubated

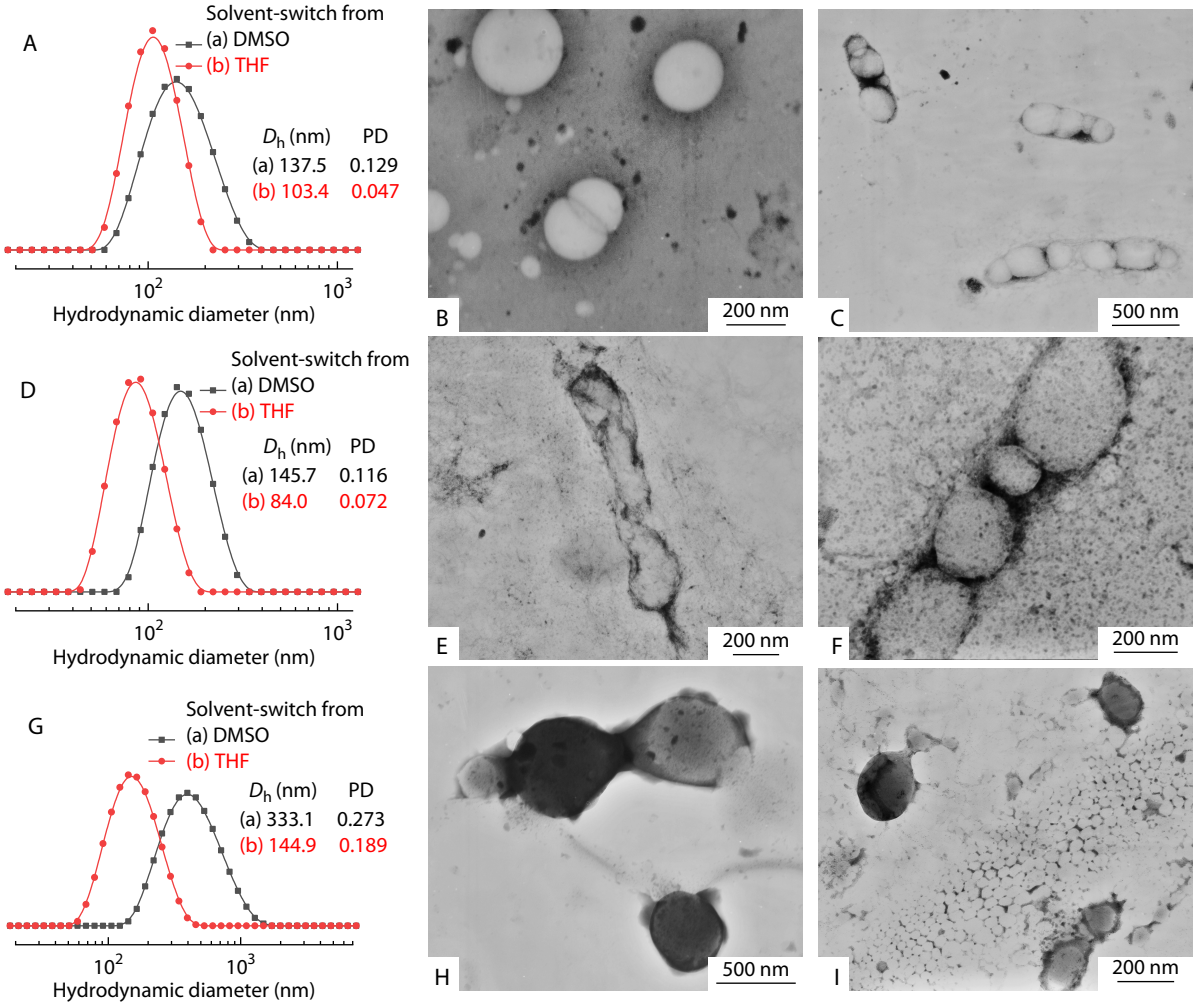

Fig. 1 DLS and TEM studies of polymersomes prepared by solvent-switch method. (A), (D), and (G) are DLS curves of polymersomes self-assembled from PEO_{43}-*b*-P(CL_{45}-*stat*-$CTCL_{25}$), PEO_{43}-*b*-P(CL_{108}-*stat*-$CTCL_{16}$), and PEO_{43}-*b*-$PCTCL_4$-*b*-PCL_{79}, respectively; (B), (E), (H) are TEM images of polymersomes that were prepared by using DMSO as initial solvent, and (C), (F), (I) were prepared with the same method where THF was used as initial solvent.

https://doi.org/10.1007/s10118-022-2683-7

in Tris buffer (0.01 mol/L, pH 7.4) at 37 °C. As the DLS curves indicate, the D_h and PD of all proposed polymersomes remain stable under physiological conditions for more than 120 h (Figs. S18 and S19 in ESI). This demonstrates potential for their application as drug delivery vehicles for *in vivo* applications.

MesoDyn Simulations of the Phase Separation within Polymersome Membranes

For the polymersomes with incompatible compositions within the membrane, it is a common phenomenon to gradually induce phase separation. Since PCTCL and PCL have different physicochemical properties, they are not fully compatible with each other; so, phase separation between the two components will occur during self-assembly and cross-linking.

To investigate into the phase separation behavior within polymersome membrane, we used the module of MesoDyn in the software of *Materials Studio*. Such computer simulations were employed because the membrane phase separation occurs within a range of 100 nm; this makes it difficult to visualize such properties by experiments (such as TEM).[41,42] MesoDyn is a simulation method based on mean-field density functional theory. Polymer properties can be calculated by transforming the real molecules to coarse-grained Gaussian chains. First, three molecular models for repeating unit of PCTCL, PCL and PEO were created (Fig. S20 in ESI). Secondly, the corresponding physicochemical properties of the polymers were calculated using the module of Synthia (Table S2 in ESI). Then, the Flory-Huggins parameters between each pair of chemical structures were determined.

By further using the module of MesoDyn, phase separation within the polymersome membrane was simulated. As shown in Fig. S21 (in ESI), two phases (PCL and PCTCL) show interconnection behavior in the most cases, however, when the two components have similar bead numbers, phase structures will become layer-like, and when the proportion of the two components differs greatly, the phase with the lesser portion will tend to form spherical phases and disperse in the major phase.

Owing to the photo-cross-linkable character of the PCTCL moieties and the chain flexibility of the polymers, the cycloaddition procedures will also initiate shear between the polymer chains. In this way, shear was added to the MesoDyn system to investigate the phase separation when photo-cross-linking is initiated. As can be observed in Fig. S22 (in ESI), the phase patterns become more regulated and oriented when applying a shear.

Afterwards, the phase separation of all three polymer compositions (PEO, PCL and PCTCL) was evaluated using the same method. In contrast to the statistical polymer membrane, for the triblock copolymer, it is important to include the hydrophilic coronas in the MesoDyn simulations to check the possible influences by molecular architecture, therefore, PEO was introduced to the MesoDyn system. Under the same simulation procedures, the phase separation behaviour between hydrophilic PEO and hydrophobic blocks were investigated. As shown in Fig. S23 (in ESI), beads of PCTCL and PEO both show clear boundaries with PCL, and thus a well-defined layer-like structure can be obtained. In contrast, PEO and PCTCL only show single-phase structures at interfaces with PCL phase, and these two polymers seem mostly compatible with each other. Since in reality the structures are immersed in water, to stabilize the morphology of polymersomes, the hydrophilic PEO moieties will preferably disperse in water, so as to further guide the phase separation between PEO and PCTCL. In this way, the triblock copolymer, PEO-*b*-PCTCL-*b*-PCL self-assembles into a polymersome with PEO as coronas and with a membrane of a continuous PCL capsule covered by PCTCL moieties.

Finally, by using the characteristic ratio of each polymeric moiety, the three polymers can be converted into polymers with different bead numbers: $PEO_{8.6}$-*b*-P($CL_{7.8}$-*stat*-$CTCL_{3.1}$), $PEO_{8.6}$-*b*-P(CL_{19}-*stat*-$CTCL_{2.0}$) and $PEO_{8.6}$-*b*-$PCTCL_{0.50}$-*b*-PCL_{14}. By referring to the phase graph, $PEO_{8.6}$-*b*-P($CL_{7.8}$-*stat*-$CTCL_{3.1}$) has a membrane with a bicontinuous phase structure; $PEO_{8.6}$-*b*-P(CL_{19}-*stat*-$CTCL_{2.0}$) has a membrane with an island-like phase structure. By further applying photo-cross-linking, the bicontinuous phase structure turns into oriented layer-like structures, and the island-like phase structures turn into cylindrical phase structures. Regarding the triblock copolymer vesicles, due to the hydrophilicity of PEO, PCTCL moieties tend to distribute between PEO and hydrophobic PCL core, thus forming a longitudinal phase-separated structure.

These simulations indicate that the polymersome membrane phase structures can be altered by employing polymers with membrane-forming blocks of either statistical compositions or a block composition, in addition to the photo-cross-linking degree. Such insights into the tunability of the membrane phase structures allow more finely controlled membrane structures that meet the specific drug loading and release profiles that are required to achieve an optimal drug release behavior.

Controlled Drug Release of Polymersomes

Small molecules are widely-used in biomedical applications, and polymersomes are used as their carriers to boost the delivery efficiency.[43] By using a typical anticancer drug, doxorubicin (DOX), we evaluated the control of drug release by either adjusting the membrane phase structure or by tuning the photo-cross-linking degree of the PCTCL moieties in the membrane.

As we have confirmed in our previous work, the polymersome membrane solely composed of PCTCL is rather leaky to DOX; however, the release rate can be reduced by photo-cross-linking.[27] In this way, by first introducing semi-crystalline PCL moieties into the polymersome membrane and then performing photo-cross-linking, diversified release behaviors of DOX can be obtained, which further expands the possible biomedical suitability of PCTCL-based polymersomes.

First, polymersomes with different membrane-forming blocks were used for comparing the drug release rate without membrane-cross-linking. As shown in Fig. 2, due to the intrinsic amorphous character of PCTCL and the semi-crystalline character of PCL, PEO-*b*-PCTCL and PEO-*b*-PCL polymersomes with homogeneous membranes show the highest and lowest drug release rate, respectively.

Then, for PEO-*b*-P(CL-*stat*-CTCL) polymersomes with an inhomogeneous membrane that is made of statistical compositions, the release rate was significantly reduced with the increased percentage of PCL moieties. As for PEO-*b*-PCTCL-*b*-

https://doi.org/10.1007/s10118-022-2683-7

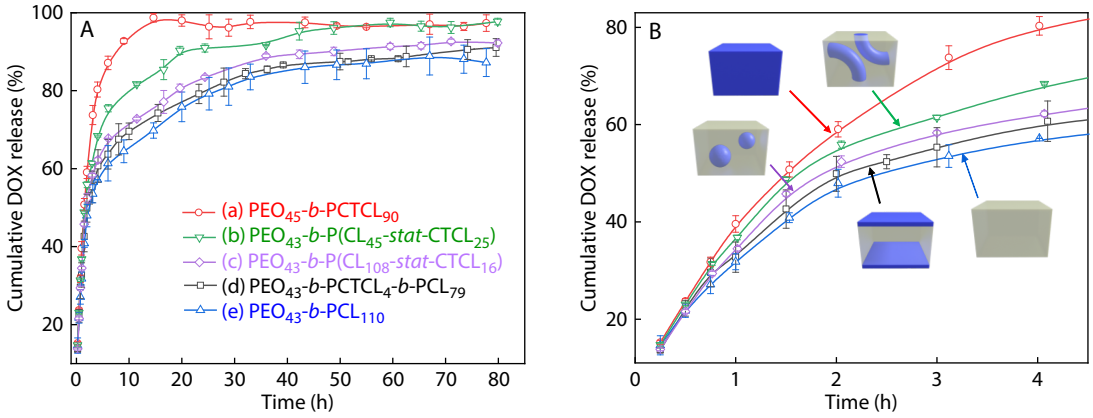

Fig. 2 Drug release curves of polymersomes with different membrane phase patterns. (A) Overall drug release profiles; (B) The enlargement of (A) and the corresponding membrane phase patterns, revealing the drug release kinetics resulted from different membrane compositions. The blue phase indicates the patterns formed by PCTCL. As the connection of PCTCL phases gradually forms, the drug release rate increases accordingly.

PCL polymersomes with an inhomogeneous membrane that is made of block compositions, the chain architecture where PCL moieties can locate securely within the core of membrane, the drug release rate can reach a slow release rate similar to that of PEO-*b*-PCL polymersomes.

Then, the drug release profiles from photo-cross-linked polymersomes, that were obtained from triblock copolymers using the solvent-switch method, were investigated. As expected, the drug release rate was significantly lowered when increasing the UV irradiation time (Fig. 3). This is consistent with the membrane becoming more compact upon photo-cross-linking.

However, the polymersomes with membranes of statistical compositions show a different tendency in the release test. After 80 min of UV irradiation, the drug release rate was significantly promoted in comparison to that with only 15 min of UV irradiation for both PEO_{43}-*b*-P(CL_{45}-*stat*-$CTCL_{25}$) and PEO_{43}-*b*-P(CL_{108}-*stat*-$CTCL_{16}$) polymersomes (Fig. 4). The experimental results are consistent with the theoretical simulation results. Since photo-cross-linking process leads to more ori-

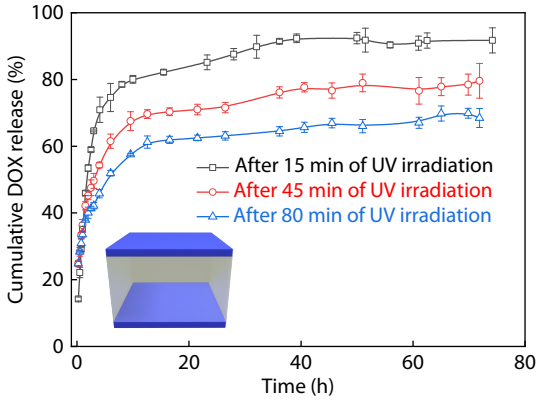

Fig. 3 Drug release profiles and membrane phase pattern of polymersomes that were obtained from triblock copolymers using the solvent-switch method, with block membrane composition with different UV-cross-linking time. The permeable PCTCL (blue) phase is well separated by the PCL phase so as to significantly reduce the release rate and prevent re-orientation of PCTCL phases upon cross-linking.

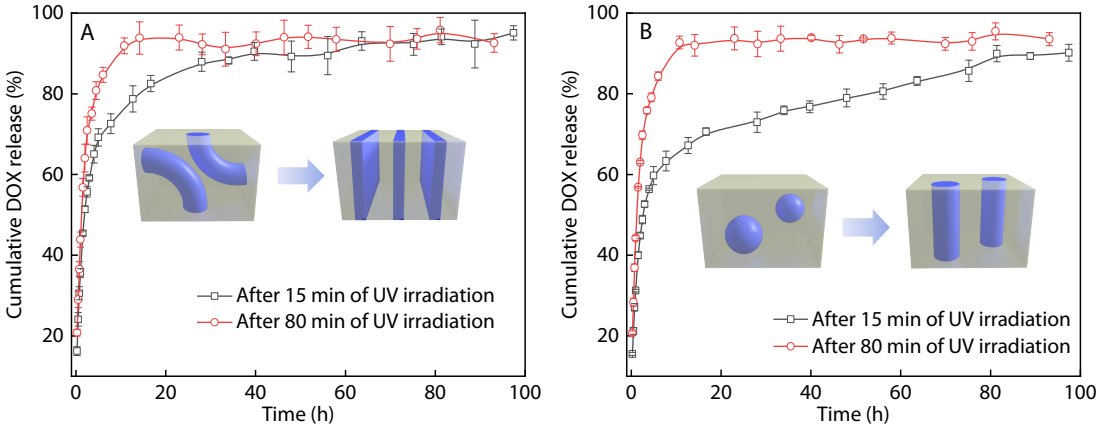

Fig. 4 Drug release profiles and membrane phase patterns of polymersomes with statistical membrane compositions after UV-cross-linking. (A) Drug release from PEO_{43}-*b*-P(CL_{45}-*stat*-$CTCL_{25}$) polymersomes; (B) Drug release from PEO_{43}-*b*-P(CL_{108}-*stat*-$CTCL_{16}$) polymersomes. The blue phase indicates the pattern formed by PCTCL within the membrane. Along with the increase of irradiation time, the phase separation patterns gradually switched.

https://doi.org/10.1007/s10118-022-2683-7

ented phase patterns, the release rate actually increased as the cross-linking time significantly prolonged. Subsequently, re-organization of the phase pattern within polymersome membrane gradually occurred during the cross-linking process. However, for the polymersomes with block compositions within the membrane, the re-organization effect was not as strong as the compacting effect from photo-cross-linking.

The drug loading efficiencies of all loading experiments were calculated and summarized in Table S3 (in ESI). The overall loading efficiencies are around 30%, which implies good potentials for these polymersomes to be used as drug loading and release vehicles in various biomedical applications.

By combination of both controlling the molecular architecture and photo-cross-linking degree, in reference of the simulation results, the drug release behavior can be finely tuned due to the control of membrane phase patterns, which offers a potent strategy toward refined design of vehicles for programmed release of drugs.

CONCLUSIONS

We designed polymersomes with inhomogeneous membranes and elucidated ways to control membrane phase separation, which allowed accurate control for programmed drug release. Three polymersomes were synthesized that were based on polymers with different hydrophobic chains, PEO_{43}-*b*-P(CL_{45}-*stat*-$CTCL_{25}$), PEO_{43}-*b*-P(CL_{108}-*stat*-$CTCL_{16}$), and PEO_{43}-*b*-$PCTCL_4$-*b*-PCL_{79}, which introduced crystalline PCL moiety to adjust the high permeability resulting from the amorphous PCTCL moieties in the membrane. With the assistance of MesoDyn simulations and doxorubicin release tests, we confirmed that the membrane permeability is related to the membrane phase separation. Overall, control over membrane phase separation was achieved by employing different polymer architectures, as well as photo-cross-linking, which allowed these polymersomes to accurately release small molecular drugs in a controlled way. This study shed light on the development of drug delivery and release vehicles with programmed release capabilities.

NOTES

The authors declare no competing financial interest.

Electronic Supplementary Information

Electronic supplementary information (ESI) is available free of charge in the online version of this article at http://doi.org/10.1007/s10118-022-2683-7.

ACKNOWLEDGMENTS

J. D. is financially supported by the National Natural Science Fund for Distinguished Young Scholars (No. 21925505) and Shanghai International Scientific Collaboration Fund (No. 21520710100). E. J. C. is supported by the National Natural Science Foundation of China (No. 22101207), the China Postdoctoral Science Foundation (No. 2020M671197) and International Postdoctoral Exchange Fellowship Program.

REFERENCES

1 Tibbitt, M. W.; Dahlman, J. E.; Langer, R. Emerging frontiers in drug delivery. *J. Am. Chem. Soc.* **2016**, *138*, 704–717.
2 Dou, Y.; Li, C. W.; Li, L. L.; Guo, J. W.; Zhang, J. X. Bioresponsive drug delivery systems for the treatment of inflammatory diseases. *J. Control. Release* **2020**, *327*, 641–666.
3 Hassan, S.; Prakash, G.; Ozturk, A. B.; Saghazadeh, S.; Sohail, M. F.; Seo, J.; Dokmeci, M. R.; Zhang, Y. S.; Khademhosseini, A. Evolution and clinical translation of drug delivery nanomaterials. *Nano Today* **2017**, *15*, 91–106.
4 Prasanna, A.; Pooja, R.; Suchithra, V.; Ravikumar, A.; Gupta, P. K.; Niranjan, V. Smart drug delivery systems for cancer treatment using nanomaterials. *Mater. Today: Proc.* **2018**, *5*, 21047–21054.
5 Rasheed, T.; Nabeel, F.; Raza, A.; Bilal, M.; Iqbal, H. M. N. Biomimetic nanostructures/cues as drug delivery systems: a review. *Mater. Today Chem.* **2019**, *13*, 147–157.
6 Jiang, J.; Zhuravlev, E.; Hu, W. B.; Schick, C.; Zhou, D. S. The effect of self-nucleation on isothermal crystallization kinetics of poly(butylene succinate) (PBS) investigated by differential fast scanning calorimetry. *Chinese J. Polym. Sci.* **2017**, *35*, 1009–1019.
7 Sharma, A. K.; Prasher, P.; Aljabali, A. A.; Mishra, V.; Gandhi, H.; Kumar, S.; Mutalik, S.; Chellappan, D. K.; Tambuwala, M. M.; Dua, K.; Kapoor, D. N. Emerging era of "somes": polymersomes as versatile drug delivery carrier for cancer diagnostics and therapy. *Drug Deliv. Transl. Res.* **2020**, *10*, 1171–1190.
8 Lee, J. S.; Feijen, J. Polymersomes for drug delivery: design, formation and characterization. *J. Control. Release* **2012**, *161*, 473–483.
9 Liu, D. Q.; Sun, H.; Xiao, Y. F.; Chen, S.; Cornel, E. J.; Zhu, Y. Q.; Du, J. Z. Design principles, synthesis and biomedical applications of polymer vesicles with inhomogeneous membranes. *J. Control. Release* **2020**, *326*, 365–386.
10 Fenton, O. S.; Olafson, K. N.; Pillai, P. S.; Mitchell, M. J.; Langer, R. Advances in biomaterials for drug delivery. *Adv. Mater.* **2018**, *30*, 1705328.
11 Allen, T. M.; Cullis, P. R. Drug delivery systems: Entering the mainstream. *Science* **2004**, *303*, 1818–1822.
12 Felice, B.; Prabhakaran, M. P.; Rodriguez, A. P.; Ramakrishna, S. Drug delivery vehicles on a nano-engineering perspective. *Mater. Sci. Eng., C* **2014**, *41*, 178–195.
13 Sun, R.; Qiu, N. S.; Shen, Y. Q. Polymeric cancer nanomedicines: Challenge and development. *Acta Polymerica Sinica* (in Chinese) **2019**, *50*, 588–601.
14 Davoodi, P.; Lee, L. Y.; Xu, Q. X.; Sunil, V.; Sun, Y. J.; Soh, S.; Wang, C. H. Drug delivery systems for programmed and on-demand release. *Adv. Drug Deliv. Rev.* **2018**, *132*, 104–138.
15 Uhrich, K. E.; Cannizzaro, S. M.; Langer, R. S.; Shakesheff, K. M. Polymeric systems for controlled drug release. *Chem. Rev.* **1999**, *99*, 3181–3198.
16 He, F.; Zhang, M. J.; Wang, W.; Cai, Q. W.; Su, Y. Y.; Liu, Z.; Faraj, Y.; Ju, X. J.; Xie, R.; Chu, L. Y. Designable polymeric microparticles from droplet microfluidics for controlled drug release. *Adv. Mater. Technol.* **2019**, *4*, 1800687.
17 Le Meins, J. F.; Sandre, O.; Lecommandoux, S. Recent trends in the tuning of polymersomes' membrane properties. *Eur. Phys. J. E* **2011**, *34*, 14.
18 Chidanguro, T.; Ghimire, E.; Liu, C. H.; Simon, Y. C. Polymersomes: breaking the glass ceiling. *Small* **2018**, *14*, 1802734.
19 Du, F. F.; Bobbala, S.; Yi, S. J.; Scott, E. A. Sequential intracellular release of water-soluble cargos from shell-crosslinked polymersomes. *J. Control. Rel.* **2018**, *282*, 90–100.

20 Miller, A. J.; Pearce, A. K.; Foster, J. C.; O'Reilly, R. K. Probing and tuning the permeability of polymersomes. *ACS Cent. Sci.* **2021**, *7*, 30–38.

21 Larranaga, A.; Lomora, M.; Sarasua, J. R.; Palivan, C. G.; Pandit, A. Polymer capsules as micro-/nanoreactors for therapeutic applications: current strategies to control membrane permeability. *Prog. Mater. Sci.* **2017**, *90*, 325–357.

22 Leong, J.; Teo, J. Y.; Aakalu, V. K.; Yang, Y. Y.; Kong, H. Engineering polymersomes for diagnostics and therapy. *Adv. Healthc. Mater.* **2018**, *7*, 1701276.

23 Yao, C. Z.; Wang, X. R.; Hu, J. M.; Liu, S. Y. Cooperative modulation of bilayer permeability and microstructures of polymersomes. *Acta Polymerica Sinica* (in Chinese) **2019**, *50*, 553–566.

24 Chang, H. Y.; Lin, Y. L.; Sheng, Y. J.; Tsao, H. K. Structural characteristics and fusion pathways of onion-like multilayered polymersome formed by amphiphilic comb-like graft copolymers. *Macromolecules* **2013**, *46*, 5644–5656.

25 Yan, Q.; Wang, J. B.; Yin, Y. W.; Yuan, J. Y. Breathing polymersomes: CO_2-tuning membrane permeability for size-selective release, separation, and reaction. *Angew. Chem. Int. Ed.* **2013**, *52*, 5070–5073.

26 Thambi, T.; Deepagan, V. G.; Ko, H.; Suh, Y. D.; Yi, G. R.; Lee, J. Y.; Lee, D. S.; Park, J. H. Biostable and bioreducible polymersomes for intracellular delivery of doxorubicin. *Polym. Chem.* **2014**, *5*, 4627–4634.

27 Chen, S.; Qin, J. L.; Du, J. Z. Two principles for polymersomes with ultrahigh biomacromolecular loading efficiencies: acid-induced adsorption and affinity-enhanced attraction. *Macromolecules* **2020**, *53*, 3978–3993.

28 Varlas, S.; Foster, J. C.; Georgiou, P. G.; Keogh, R.; Husband, J. T.; Williams, D. S.; O'Reilly, R. K. Tuning the membrane permeability of polymersome nanoreactors developed by aqueous emulsion polymerization-induced self-assembly. *Nanoscale* **2019**, *11*, 12643–12654.

29 Gaitzsch, J.; Hirschi, S.; Freimann, S.; Fotiadis, D.; Meier, W. Directed insertion of light-activated proteorhodopsin into asymmetric polymersomes from an ABC block copolymer. *Nano Lett.* **2019**, *19*, 2503–2508.

30 Kumar, M.; Grzelakowski, M.; Zilles, J.; Clark, M.; Meier, W. Highly permeable polymeric membranes based on the incorporation of the functional water channel protein Aquaporin Z. *Proc. Natl. Acad. Sci. U. S. A.* **2007**, *104*, 20719–20724.

31 Chen, S.; Lin, S.; Xi, Y. J.; Xiao, Y. F.; Du, J. Z. Polymersomes with inhomogeneous membranes, asymmetrical coronas and fused membranes and coronas. *Chin. Sci. Bull.* **2020**, *65*, 2615–2626.

32 Wang, F. Y. K.; Xiao, J. G.; Chen, S.; Sun, H.; Yang, B.; Jiang, J. H.; Zhou, X.; Du, J. Z. Polymer vesicles: Modular platforms for cancer theranostics. *Adv. Mater.* **2018**, *30*, 1705674.

33 Xiao, Y. F.; Sun, H.; Du, J. Z. Sugar-breathing glycopolymersomes for regulating glucose level. *J. Am. Chem. Soc.* **2017**, *139*, 7640–7647.

34 Wang, F. Y. K.; Gao, J. Y.; Xiao, J. G.; Du, J. Z. Dually gated polymersomes for gene delivery. *Nano Lett.* **2018**, *18*, 5562–5568.

35 Zhu, Y. Q.; Wang, F. Y. K.; Zhang, C.; Du, J. Z. Preparation and mechanism insight of nuclear envelope-like polymer vesicles for facile loading of biomacromolecules and enhanced biocatalytic activity. *ACS Nano* **2014**, *8*, 6644–6654.

36 Yang, Y. Y.; Chen, L. S.; Sun, M.; Wang, C. Y.; Fan, Z.; Du, J. Z. Biodegradable polypeptide-based vesicles with intrinsic blue fluorescence for antibacterial visualization. *Chinese J. Polym. Sci.* **2021**, *39*, 1412–1420.

37 Liang, R.; Chen, Y. C.; Zhang, C. Q.; Yin, J.; Liu, X. L.; Wang, L. K.; Kong, R.; Feng, X.; Yang, J. J. Crystallization behavior of biodegradable poly(ethylene adipate) modulated by a benign nucleating agent: zinc phenylphosphonate. *Chinese J. Polym. Sci.* **2017**, *35*, 558–568.

38 Bicerano, J. Prediction of the properties of polymers from their structures. *J. Macromol. Sci., Rev. Macromol. Chem. Phys.* **1996**, *C36*, 161–196.

39 Altevogt, P.; Evers, O. A.; Fraaije, J. G. E. M.; Maurits, N. M.; van Vlimmeren, B. A. C. The MesoDyn project: software for mesoscale chemical engineering. *J. Mol. Struct.: THEOCHEM* **1999**, *463*, 139–143.

40 Jiang, J. H.; Zhu, Y. Q.; Du, J. Z. Challenges and perspective on ring-opening polymerization-induced self-assembly. *Acta Chim. Sin.* **2020**, *78*, 719–724.

41 Gartner, T. E.; Jayaraman, A. Modeling and simulations of polymers: a roadmap. *Macromolecules* **2019**, *52*, 755–786.

42 Zhu, Y. L.; Lu, Z. Y. Dynamics simulations of supramolecular and polymeric self-assemblies. *Acta Polymerica Sinica* (in Chinese) **2021,** *52*, 884–897.

43 Zhao, R.; Zhou, Y. J.; Jia, K. C.; Yang, J.; Perrier, S.; Huang, F. H. Fluorescent supramolecular polymersomes based on pillararene/paraquat molecular recognition for pH-controlled drug release. *Chinese J. Polym. Sci.* **2020**, *38*, 1–8.

https://doi.org/10.1007/s10118-022-2683-7